Study of Surface Dynamics during Laser Polishing of Glass

Fidel Vega, Jesús Armengol, Núria Lupón, and Ferran Laguarta

Center for Sensors, Instruments and Systems Development (CD6)[1]
Departament d'Òptica i Optometria
Universitat Politècnica de Catalunya
C. Violinista Vellsolà 37, 08222 Terrassa, Spain

ABSTRACT

Laser heating of glass samples is a simple and versatile method for obtaining polished surfaces of optical quality. Since laser beam intensity non-uniformity can translate into significant variations in the induced surface temperature, the success of the laser surface-polishing process strongly depends on obtaining uniform intensity profiles or flat-top distributions at the sample plane.

In this paper we present a comparison between large-area CO_2 laser-polishing experiments carried out in optical glass substrates following two different approaches:
1) A reshaped beam obtained by an active integration method is swept over the glass surface
2) A static beam reshaped by means of both a multifaceted mirror and a square pipe light guide is applied.

The efficiency of each procedure in reducing both the *roughness* and the *waviness* of the glass surface texture is discussed. Moreover, it is shown that both approaches can induce relief structures such as *ripples* (approach (1) with strongly focused beams), and *hill-shape* local deformations (approach (2)). The comparison of these results allow us to clarify the role of the induced lateral surface thermal gradients, the initial surface texture and the laser beam non-uniformity in the dynamics of the glass surface during the laser polishing process.

Keywords: Laser polishing, laser beam integration, thermal assessment, roughness measurements

1. INTRODUCTION

The processing of materials based on the melting or softening of a thin surface layer has been used to enhance or modify the surface properties and, in particular, to polish rough surfaces[1,2]. The polishing or, equivalently, the decrease in surface roughness occurs because of a surface tension driven flow in the molten or softened layer. This layer must be at least as deep as the peak-to-valley initial surface roughness. Moreover, the polishing flow occurs only if the surface layer is kept molten or softened for long enough.

Laser polishing of glass[3,4] is an extraordinarily attractive possibility from an industrial point of view since it would improve the production efficiency of standard components and at the same time allow the automation of the polishing process. Moreover, it requires no mechanical abrasives or surfaced-adapted polishing tools. This technique may be especially suitable for difficult to access surfaces and for obtaining non-spherical and non-revolution optical polished surfaces, which are very difficult and sometimes even impossible to polish using traditional techniques.

Commonly, laser surface treatments require both the contribution of a large amount of energy on the surface and a controlled and customized beam intensity distribution at the sample plane. These requirements have extended the use of unstable cavity laser sources that provide high-power almost pure transverse monomode beams with high spatial coherence. In addition, both metallic light guides[5] and multifaceted laser beam integrating mirrors[6,7] are widely used to obtain flat-top intensity profiles in high-power applications. However, integration of coherent beams results in an intensity profile that shows a sharp contrast because of the interferential effects produced by the superposition of the different portions of the segmented wavefront. In

[1] For further information - email: fvega@oo.upc.es

Part of the EUROPTO Conference on Computer-Controlled Microshaping • Munich, Germany • June 1999
SPIE Vol. 3822 • 0277-786X/99/$10.00

laser applications involving materials with a low thermal conductivity such as glass, the above-mentioned effect translates into a non-uniform temperature distribution with steep transverse thermal gradients that could induce the sample to crack.

The goal of this paper is to study the dynamics of the laser polishing process of optical glass by using integrated intensity distributions obtained using two different approaches. The first consists of applying a static laser beam reshaped by means of either a multifaceted mirror or a square copper guide, while in the second approach the beam is integrated by means of an active method[8] and is swept over the sample surface. The comparison between the two methods together with thermal simulations of the laser heating process allow us to clarify the role of the induced lateral surface thermal gradients, the initial surface texture and the laser beam non-uniformity in the dynamics of the glass surface during the laser polishing process.

2. EXPERIMENTS

The samples treated were circular pieces (diameter = 80 mm) of white crown optical glass (B-270 and TRC-33) with concave and spherical surfaces of curvature radius ranging from 60 to 225 mm. Samples with different initial rms surface roughness were studied (up to a maximum of 500 nm rms).

Since glass does not exhibit a well-defined fusion-phase transition, a gradual increase in its temperature induces a progressive decrease in its viscosity and a consequent increase in its ability to flow. To polish, temperature values on the glass surface must typically be above 1000°C, since only for these values is the glass viscosity coefficient small enough ($\leq 10^4$ Pa*s) for a surface tension driven mass flow to be established. Moreover, to avoid overall deformation, temperature values in the bulk of the sample must be kept below the glass softening temperature (≈650°C).

When glass undergoes laser treatment, depth thermal gradients always appear because of its high absorption and its low thermal diffusivity. As the thermal expansion coefficient depends on temperature, these steep depth thermal gradients cause internal stresses in a treated glass sample and might make it crack[3]. These undesirable effects worsen when the temperature is around the transformation point (T_g = 530°C), since the thermal expansion coefficient increases suddenly at this point. Therefore, samples must be preheated to a temperature slightly higher than T_g. Also, after the laser treatment, during cooling, the temperature of the sample must pass through the transformation point in a controlled way, following a typical annealing cycle. To satisfy these needs, the laser treatment is always carried out in an oven.

2.1 Intensity distribution.

To minimize the occurrence of steep transverse thermal gradients on the glass surface a uniform laser intensity distribution is needed. Such a distribution is usually obtained by means of a suitable integration system. In this paper we present results obtained by using two different approaches to integrate the laser beam.

The first one (referred to hereafter as the static approach) consists of irradiating the sample by using a static beam that has been reshaped by using either a multifaceted or a square pipe light guide (kaleidoscope). The second procedure uses an active integration method to obtain a strip beam that is swept over the glass surface at constant speed. This approach will be referred to hereafter as the scanning approach. In the following, the experimental setups are described.

The CO_2 laser (λ = 10.6 μm) delivers a highly spatially coherent beam with an intensity distribution corresponding to the TEM^*_{01} mode. The multifaceted mirror is spherical, molybdenum-coated, and 6x6 faceted (focal length = 500 mm) whereas the kaleidoscope is a 70 mm length, 4x4 mm^2 copper pipe light guide. The former induces beam uniformization because each facet reflects a part of the collimated incoming beam and these reflected beamlets overlap at the focal plane of the mirror. The size of the laser spot in this plane is 80 mm^2 and is limited by the size of the flat facets of the mirror. Further details can be found elsewhere[9]. The pipe light guide integrates an incoming diverging beam by means of multiple reflections from the inside walls of the pipe. A ZnSe spherical lens focuses the CO_2 beam at the entrance face of the guide. This beam undergoes several reflections as it passes through the guide. In this case the best integration plane is achieved at the 4x4 mm^2 square exit face of the pipe. Then, to irradiate larger areas using either the multifaceted mirror or the light guide, an optical system must be used to image, with the required dimensions, the best integration plane onto the sample surface.

The scanning approach is based on an active integration technique that has been described in detail in Ref. 8. It consists of a high quality gold-coated infrared mirror formed by two separate facets, one of which is able to vibrate under the action of a piezoelectric transducer. After reflection, the laser intensity distribution is divided into two symmetric distributions that are forced to partially overlap in order to obtain a more uniform intensity distribution. Following reflection in the two-faceted

mirror, an imaging system is used to obtain a strip beam at the sample plane. When this distribution is swept over the sample surface a quite uniform intensity profile should be achieved. It is worth noting that all the above-mentioned methods perform the beam integration by means of the superposition of different portions of a segmented wavefront (i.e., beamlets). Since the laser beam is highly spatially coherent the overlapping of the beamlets results in a real non-uniform intensity distribution that shows sharp contrast interferential effects.

The intensity pattern obtained with the multifaceted mirror consists of a symmetric array of intensity maxima and minima that correspond to the interference pattern mentioned above. Figure 1 shows a measured intensity profile obtained at the best integration plane with a visibility of near 100%. The characteristics of the intensity distribution (i.e. interfringe, visibility...) depend on both, the focal length and the facets size of the multifaceted mirror.

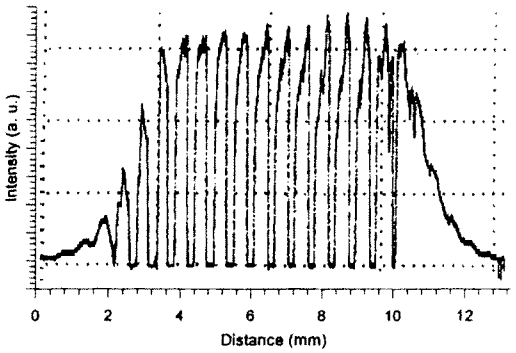

Figure 1.- Experimental laser intensity profile obtained at the sample plane when using a 6x6 multifaceted integrating mirror. In order to have a good spatial resolution the profile was recorded scanning the laser intensity distribution along a line with a pinhole positioned in front of a pyroelectric detector.

A similar pattern is obtained with a square copper guide. Figure 2 shows the imaged experimental intensity profile at the sample site. In this case the visibility is between 20% and 50%. The characteristics of the intensity distribution (i.e. interfringe, visibility...) depend on both, the dimensions of the guide (aperture and length) and the focal length of the focusing lens.

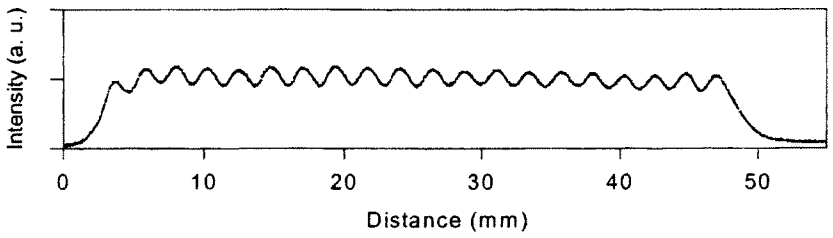

Figure 2.- Experimental intensity profile obtained at the sample site with a copper square pipe guide. The profile was recorded scanning the laser intensity distribution along a line with a pinhole positioned in front of a pyroelectric detector.

In the case of the scanning approach, the activation of the piezoelectric transducer moves one of the facets periodically ($\nu \approx$ 60-80 Hz) thus introducing a periodic phase shift between the two reflected beamlets. Consequently, the interference pattern vibrates at the same frequency and its contribution to the intensity profile is strongly reduced. This effect is shown in Fig. 3, where the experimental intensity profile obtained with the piezoelectric transducer switched on is shown. Moreover, the

combination of the two-faceted mirror and an optical imaging system results in an intensity profile with a good uniformity over a large strip beam.

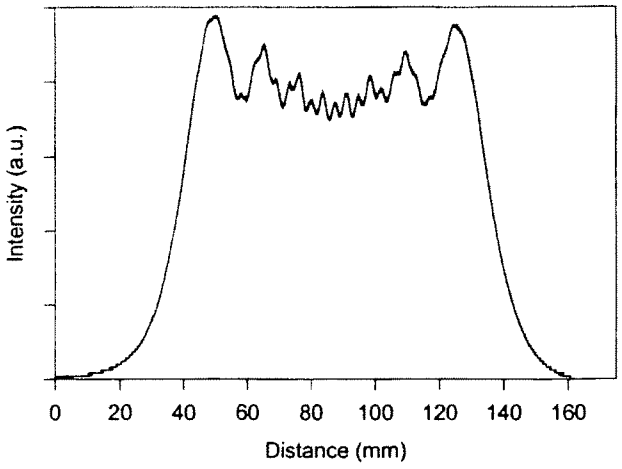

Figure 3.- Experimental intensity profile obtained along the largest dimension of the strip laser beam at the sample plane with the piezoelectric transducer switched on. The profile was recorded by using a 1.0 mm wide slit positioned in front of a pyroelectric detector and scanning the laser beam along its larger dimension.

2.2 Induced Thermal distribution

The effects of lack of uniformity in the laser beam must be taken into account since they can translate into significant variation in the induced temperature distribution of the irradiated glass sample. Such a non-uniform temperature distribution would generate steep thermal gradients (both in depth and at the surface) that would last long enough to induce irregular thermal treatment and/or undesirable effects such as permanent macroscopic surface deformation[10].

To check the above statement a 3D finite element numerical code was used to calculate the spatial and temporal temperature distribution induced in the treated samples. To obtain the sample temperature distribution T (x, y, z, t), the material is considered homogeneous in the form of a slab between the planes $z = 0$ and $z = L$, L being the sample thickness. The sample is divided into $i \cdot j \cdot l$ elements of volume $\Delta x \cdot \Delta y \cdot \Delta z$ and is taken to be at a uniform initial temperature T_o which is added to the calculated temperature. The boundary conditions are those corresponding to a thermally insulated solid, i.e., no heat flow across the boundaries is allowed. Further details of the numerical code can be found elsewhere[11]. The intensity distributions that are used to simulate the heat flow process are included in Table 1. Obviously, they are intended as an accurate reproduction of the experimental intensity profiles.

The thermal and optical parameters of the glass were taken from reference[12] and are summarized in Table 2.

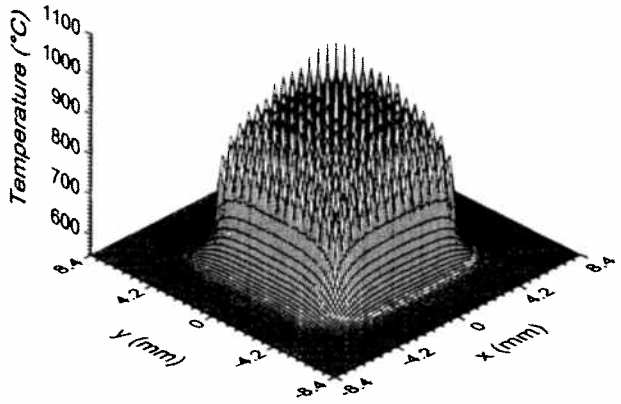

Figure 4.- Simulated surface temperature distribution on a 5 mm thick, surface infinite slab of B-270 optical glass preheated to T_0=550°C. Calculations are done using a static peak patterned intensity distribution described in table 1.

The calculated surface temperature, when applying the intensity pattern that corresponds to the static irradiation approach, shows the occurrence of thermal spikes at the surface locations where the maximum of the intensity distribution are applied (Fig. 4). This indicates that steep thermal gradients both laterally and in depth should be induced in these conditions. The thermal cycles (heating plus cooling) were calculated throughout the depth of the glass and they are shown in Fig. 5. We obtain very steep thermal gradients of about 1500°C/mm. Also, extreme differences can be noted between the cooling rates of different points on the glass surface. Values ranging from 7600°C.s^{-1} to 324°C.s^{-1} are found depending whether the surface point receives a maximum or a minimum of intensity respectively.

Table 1. Laser intensity distributions used in thermal calculations.

STATIC APPROACH	$I_o \sin^8\left(\frac{\pi}{d}x\right) \sin^8\left(\frac{\pi}{d}y\right)$	$\lvert x\rvert \le l/2,\ \lvert y\rvert \le l/2$
	0	$\lvert x\rvert \ge l/2,\ \lvert y\rvert \ge l/2$
	d= interfringe, l= beam dimensions.	
DYNAMIC APPROACH*	$\left(I_F + I_o \sin^2\left(\frac{2\pi}{\lambda}y\right)\right)\left(\sin^8\left(\frac{\pi}{\Delta x}x\right)\right)$	$0 \le x \le \Delta x,\ 0 \le y \le l'$
	0	$x \ge \Delta x,\ y \ge l'$
	$\lambda/2$= interfringe, l'= beam length, Δx= beam width.	

* Intensity distribution with the piezoelectric transducer switched off.

Table 2. Thermal and optical parameters of optical glass B-270.

ρ (kg m^{-3})	c_p (J Kg^{-1} K^{-1})	κ (W m^{-1} K^{-1})	α (m^{-1})	R
2.5×10^3	10^3	$1.047+0.001489xT^*$ (T < 900°C) 2.387 (T > 900°C)	$7.1x10^{-4}$	0.2

T^* in degrees Celsius.

Concerning lateral surface thermal gradients developed under these irradiation conditions, Fig. 6 shows the calculated thermal cycles of two neighboring surface points receiving either a maximum or a minimum of intensity (i.e., two points on the surface that are separated by one half of the interfringe). It is clear from this figure that the temperature differences between surface points are established as soon as the irradiation starts. In the calculated conditions, the maximum temperature difference obtained is higher than 200°C, which leads to a very steep lateral surface gradient (greater than 650°C/mm). However, it should be noticed that, although glass is a material with a low thermal conductivity, the lateral heat flow is high enough to average out the surface temperature differences immediately after the laser irradiation ends. In others words, both temporal and spatial thermal gradients on the glass surface will persist only during the irradiation time. This is a striking result since it shows that despite the inherent difficulty of the glass to redistribute the absorbed energy, its thermal conductivity is high enough to allow a very fast reduction (compared to the irradiation time) of the thermal gradients induced by local non-uniformity in the irradiation intensity distribution.

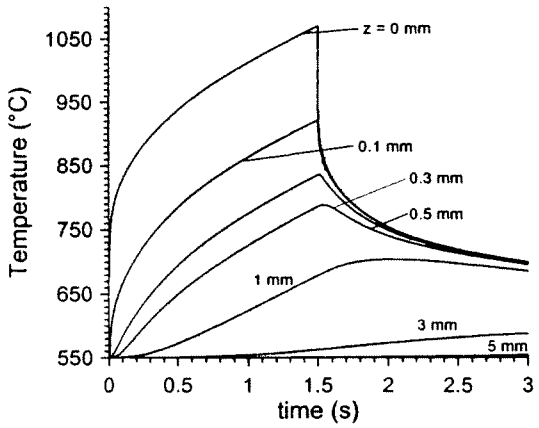

Figure 5.- Calculated in-depth temperatures as a function of time obtained in a 5mm thick, surface infinite slab of B-270 optical glass preheated to T_0=550°C. Results correspond to the same peak patterned laser intensity distribution of Fig. 4. Calculations are carried out under a surface point that receives a maximum of intensity.

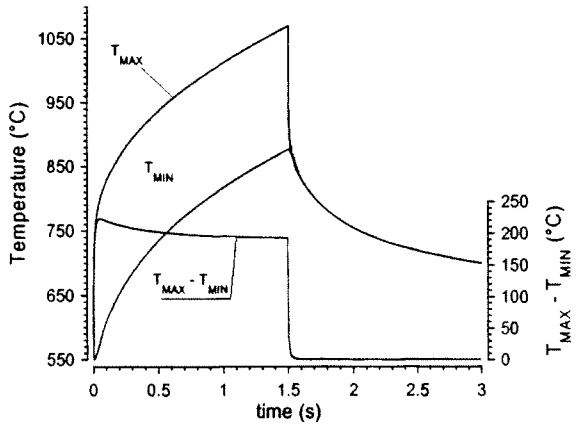

Figure 6.- Calculated surface temperature curves (scale on left) as a function of time in a 5 mm thick, surface infinite slab of B-270 optical glass preheated to T_0=550°C and irradiated with the same peak patterned laser intensity distribution of Fig. 4. Temperature curves labeled T_{MAX} and T_{MIN} correspond to adjacent surface points that receive either a maximum or a minimum of intensity. The temperature difference between these points as a function of time (curve labeled T_{MAX} - T_{MIN}, right hand axis) is also included.

In the case of the scanning approach and under the action of the piezoelectric transducer the calculated 2D surface distribution is shown in Fig. 7. The simulation is done assuming that the sweeping direction is X and including the vibration of the dynamic approach intensity distribution (see Table 1) in the Y direction (the latter induced by the action of the piezoelectric transducer). Since the surface temperature lines along the Y direction are quite straight, one can conclude that the vibration of the intensity distribution is quite effective at averaging out the contribution of the interference pattern to the resultant temperature. The calculated temperatures show that the maximum occurs at the rear of the irradiated area, since these points are those that the strip beam has completely swept. Moreover, significant transverse surface thermal gradients in the sweeping direction are obtained. These gradients are obviously steeper as the beam is more finely focused in the X direction.

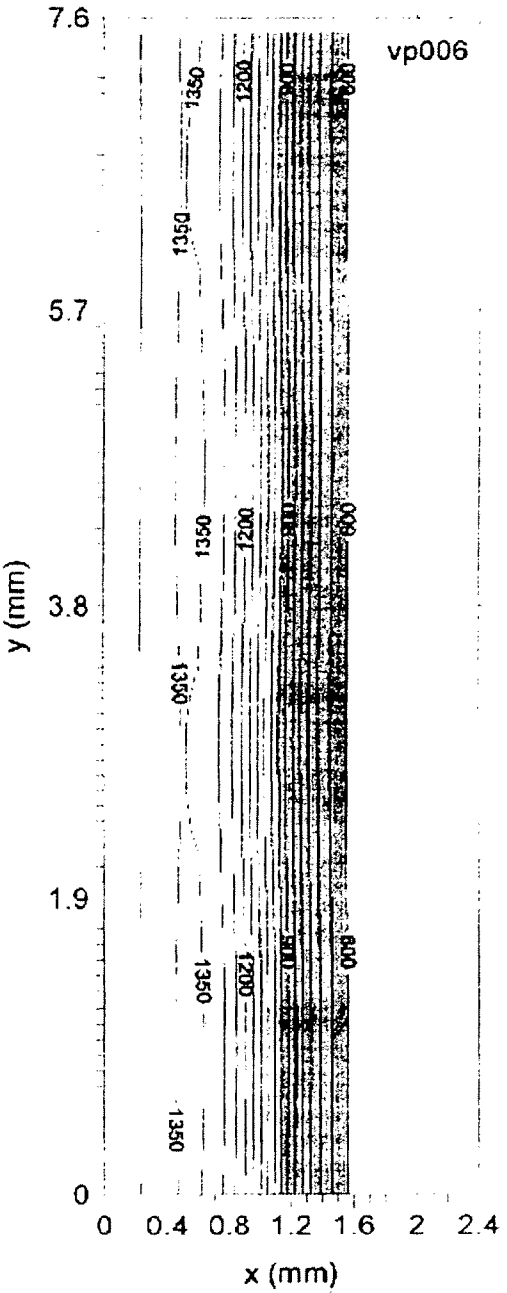

Figure 7.- Simulated surface temperature distribution on a 2.4x7.6x20mm slab of B-270 optical glass preheated to T_0=550°C. Calculations are done using a vibrating intensity distribution described in table 1.

3. EXPERIMENTAL RESULTS AND DISCUSSION

In accordance with reference 13 the surface texture of the samples (i.e., the repetitive and/or random deviations from the nominal surface that forms the three-dimensional topography of the surface) is analyzed in terms of roughness and waviness. Roughness is formed by the finer irregularities of high spatial frequency of the surface, whereas waviness refers to the more widely spaced components of the surface texture. Since roughness is considered to be superimposed on the waviness profile, each type of defect has to be measured in its own sampling length. Profile measurements are obtained with a phase-shifting optical profiler with different objectives: a 40X magnification Mirau for measuring the sample roughness with nanometric resolution, and a 2.5X objective featuring a Michelson interferometer to analyze the waviness. Since the measured surface profile includes the surface texture that is superimposed on this profile, to show the surface texture a nominal profile (exclusive of any intended surface texture) is subtracted from the measured one. Then, roughness and waviness are displayed as deviations from the nominal profile.

In general, the laser polishing process is very efficient at reducing roughness, whether we use the static approach or the scanning one. Figure 8 shows the roughness of a ground sample before and after laser treatment by using the scanning mode. Similar results were found when applying a static beam. The plot in Fig. 8(up) shows defects with a peak-to-valley height in the 260 nm range. The grinding process of the samples causes this topography. Figure 8(down) shows that after laser treatment the sample roughness has decreased by up to rms values of 1 nm with a maximum peak-to-valley height of 6 nm. It must be emphasized that this dramatic reduction in the roughness can be achieved over the entirety of a large treated area (≈5000 mm^2).

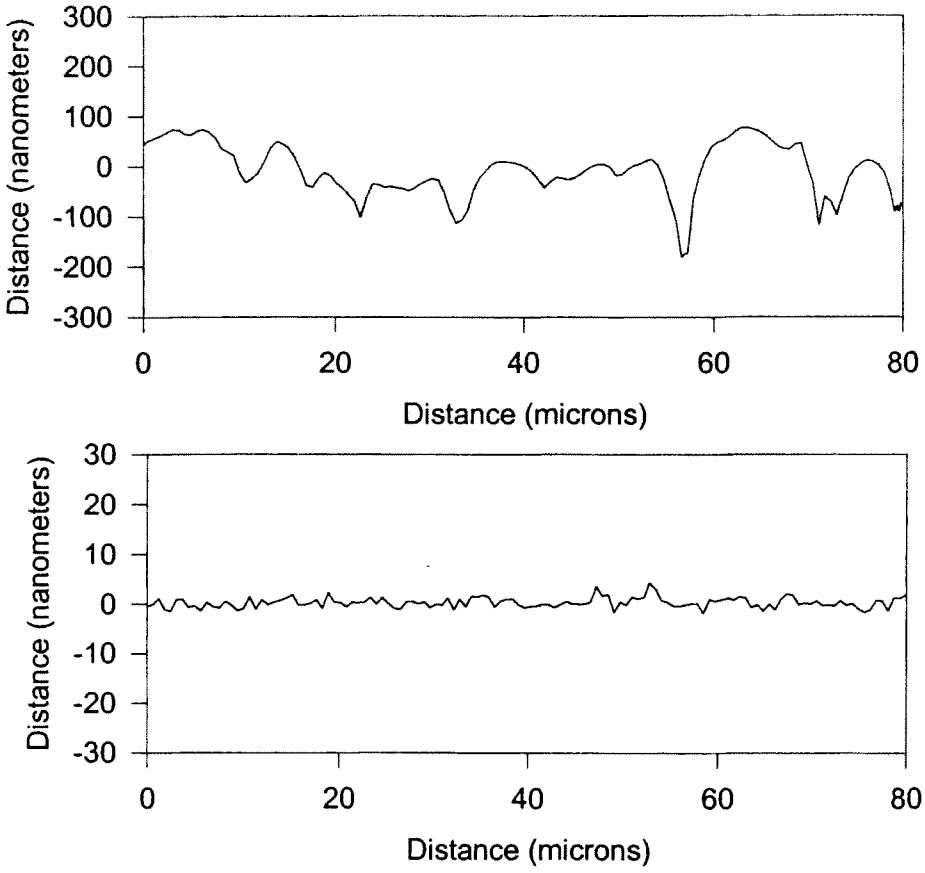

Figure 8.- Roughness profiles obtained with a 40X Mirau objective in a ground glass (TRC-33) surface (up) and after laser irradiation (down). Notice the differences between the vertical scales.

In addition, during the grinding process of the samples, randomly distributed waviness can be generated over the surface, leading to noticeable variations in the surface profile with respect to the nominal one. The ability of the laser polishing process to eliminate these defects was also investigated. Although a clear reduction in roughness was always obtained, the waviness remains almost unaffected after the laser treatment.

The difference between the high efficiency of the laser treatment in eliminating the roughness and its low capability to reduce the waviness can be understood by taking into account that the higher the slope of a defect on the surface, the higher the expected efficiency of the surface tension driven mass flow. By estimating the slope of the surface as the ratio between defect height and defect spatial length, slope values in the 10^{-2} range or higher are typically found for the roughness, whereas the larger spatial extension of the waviness leads to slopes in the 10^{-4} range. Then, the action of the surface tension during the irradiation time is not enough to reduce the waviness. Enhancement of the surface tension driven mass flow by increasing the energy deposited on the sample surface induced a macroscopic deformation of the surface figure.

The effect of the laser intensity non-uniformity on the polishing process can be seen in Fig. 9, which shows the appearance of a glass surface irradiated under the static approach. There is an "array" of surface points where a mass flow has taken place. These points undoubtedly correspond to the intensity maxima of the integrated laser distribution. The rest of the surface was not heated sufficiently to allow a significant surface flow and remains almost unaffected.

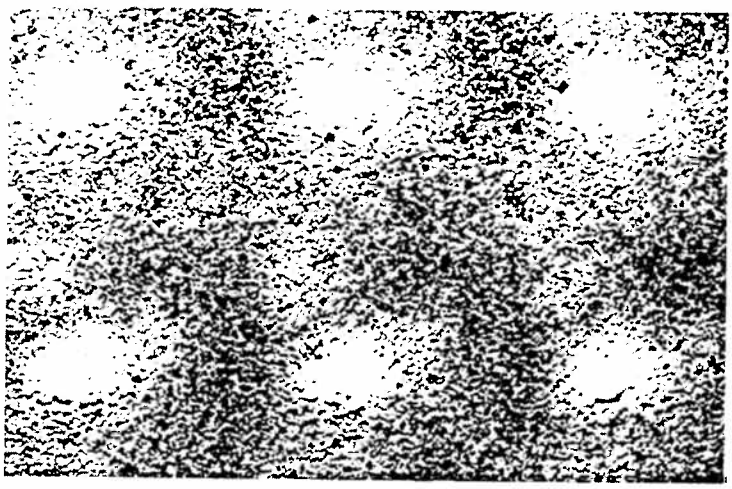

Figure 9.- Optical image of the surface of the B-270 optical glass after irradiation with a laser intensity distribution obtained by means of a 6x6 multifaceted integrating mirror. To avoid thermal cracking, the sample was preheated before the laser treatment to T_0=550ºC. The irradiation conditions are the same as in the Fig. 4.

By increasing the total energy deposited on the glass sample the coefficient of viscosity is reduced over the whole of the irradiated area, thus allowing an overall flow process with a dramatic lowering of the surface roughness. Interferometric inspection of the samples irradiated in these conditions shows that in addition to the polishing of the surface there is an associated hill-shape plastic deformation (Fig. 10), an effect that has recently been exploited to manufacture microoptical components[14,15]. This surface deformation tends to occur mainly at those points that receive a maximum of the laser intensity. Since these points become hotter, they undergo a higher thermal expansion. Moreover, because of the lowering of the density of the viscous glass with temperature, the hotter surface points tends to take on greater volume, which enhances the surface deformation process, as previously reported during irradiation of viscous liquids with Gaussian laser beams[16,17]. In the case of glass, our calculations demonstrate that the static irradiation process with a beam reshaped by using either the multifaceted mirror or the square copper pipe guide induces steep depth temperature gradients with very fast cooling rates. As a consequence, the viscoelastic expansion of the hotter surface points can become frozen as soon as the laser irradiation ends and results in the hill-shape surface observed.

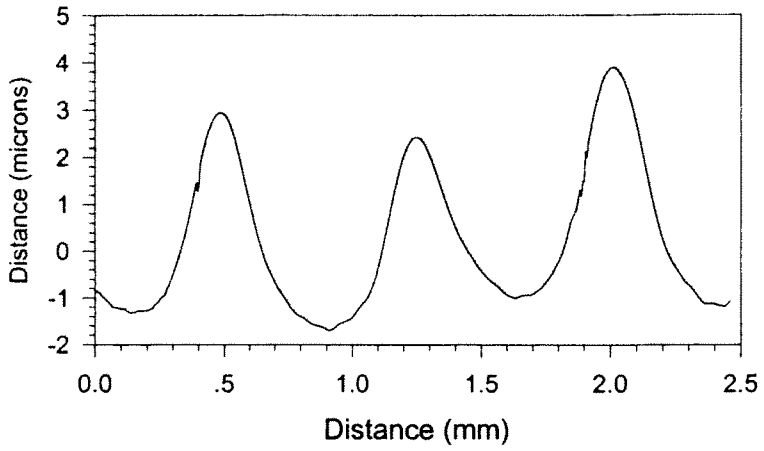

Figure 10.- Glass surface profile after irradiation with a laser intensity distribution obtained by means of a 6x6 multifaceted integrating mirror. To avoid thermal cracking, the sample was preheated before the laser treatment to T_0=550°C. The irradiation conditions are described in the text. The surface profile was obtained by using a commercial phase-shifting optical profiler with a 2.5X objective featuring a Michelson interferometer.

Finally, it must be mentioned that by using strongly focused strip beams during the sweep of the glass surface, the laser treatment can induce the formation of ripples of high amplitude. These ripples always appear perpendicular to the scanning direction and parallel to the strip laser beam (see Fig. 7). After laser irradiation we have found ripples with wavelength as high as ≈1.5 mm. Rippling effects with periodicity of the order of the laser wavelength have been widely reported during laser irradiation of metals, semiconductors and dielectric surfaces[18,19,20]. They are generated because of the interference of the incident and scattered optical waves, the latter arising from defects at the surface. Larger-scale undulations have also been observed upon laser melting and alloying of metals and semiconductors [21,22]. They are usually explained in terms of surface tension gradients that result in a surface flow. Such gradients are induced by the transverse thermal gradient between the hotter zone of the beam and the colder periphery. To check this scenario we carried out several irradiations with different widths of the laser strip beam. The energy deposited on the sample is kept constant by modifying both the laser power and the laser scan velocity. The formation of ripples was induced when the width of the laser strip beam was strongly reduced, a situation for which steep transverse thermal gradients are expected in the direction of scanning. Moreover, since it was experimentally stated that even for strongly focused beams the temperature of the points of the surface during the laser treatment is fairly uniform[23], we can discard the generation of rippling as a result of non-uniform heating of the surface.

The preceding results and discussion emphasizes that laser polishing induces a complex three- dimensional dynamics on the samples that depends on the spatially and temporally induced temperature distribution and the initial surface texture. Our results indicate that to eliminate waviness, the ability of the surface to flow should be enhanced while keeping the surface figure constant. Moreover, minimization of the transverse thermal gradients on the sample surface is of major importance for the success of the application.

4. ACKNOWLEDGMENTS

Industria de Óptica, S.A. (INDO) and Essilor International are acknowledged for financial support. This work was also supported by the Comisión Interministerial de Ciencia y Tecnología (CICYT, Ref. PTR93-0024), Spain. The authors also thank J. L. Ocaña and A. García-Beltrán for performing the numerical temperature calculations and A. Savall, J. L. Mercier, and G. Sagot for helpful discussions.

5. REFERENCES

1.- P.A. Temple, W.H. Lowdermilk, and D. Milam, "Carbon dioxide laser polishing of fused silica surfaces for increased laser-damage resistance at 1064 nm," *Appl.Opt.* **21**(18),3249-3255 (1982).

2.- A. Bosseboeuf, J. Boulmer, J. P. Budin, and D. Debarre, "Planarization of rough Si surfaces by laser annealing," *Appl. Surf. Sci.* **109-110**, 473-476 (1997).

3.- Y.M. Xiao and M. Bass, "Thermal stress limitations to laser fire polishing of glasses," *Appl.Opt.* **22**(18), 2933-2936 (1983).

4.- F. Laguarta, N. Lupon and J. Armengol, "Optical glass polishing by controlled laser surface-heat treatment," *Appl.Opt.* **33**(27), 6508-6513 (1994).

5.- R.E. Grojean, D. Feldman, J.F. Roach. "Production of flat top beam profiles for high energy lasers," *Rev. Sci. Instrum* **51**(3), 375-376 (1980).

6.- D.M. Dagenais, J.A. Woodroffe and I. Itzkan, "Optical beam shaping of a high power laser for uniform target illumination," *Appl. Opt.* **24**(5), 671-675 (1987).

7.- F.M. Dickey and B.D. O'Neil, "Multifaceted laser beam integrators: general formulation and design concepts," *Opt.Eng.***27**(11), 999-1007 (1988).

8.- J. Armengol, F. Vega, N. Lupón and F. Laguarta, "Two-faceted mirror for active integration of coherent high-power laser beams", *Appl. Opt.* **36** (3), 658-661 (1997).

9.- J. L Ocaña, A. García-Beltrán, F. Laguarta, J. Armengol, N. Lupón, and F. Vega, "Laser heat treatments driven by integrated beams: the role of irradiation non-uniformities", *Appl. Opt.* (accepted for publication).

10.- J. L Ocaña, A. García-Beltrán, F. Laguarta, J. Armengol, N. Lupón, and F. Vega, *"Analysis of the effect of optically induced local non-uniformities in laser surface treatment applications,"* Lasers in materials processing, CLEO/Europe EQUEC'96, 8-13 September 1996, Hamburg, Germany.

11.- A. García-Beltrán *"Desarrollo y validación de un modelo computacional para la predicción y caracterización de procesos de tratamiento térmico superficial de materiales con laser"*, Ph. D. Thesis. Universidad Politécnica de Madrid (1996).

12 .- *Handbook of Optical Constants of Solids*, E.D. Palik, ed., Academic Press, New York, (1985).

13.- *Surface Texture (Surface Roughness, Waviness, and Lay)* , An American National Standard ANSI/ASMEB46.1, published by The American Society of Mechanical Engineers (1985).

14.- V. P. Veiko and Y. Yakovlev, " Physical fundamentals of laser forming of microoptical components," *Opt. Eng.* **33** 3567-3571 (1994).

15.- M. Wakai, Y. Komagachi and G. Kanai, "Microlenses and microlenses array formed on a glass plate by use of a CO_2 laser." *Appl. Opt.* **37** 627-631 (1998).

16.- G. Da Costa, "Competition between capillary and gravity forces in a viscous liquid film heated by a Gaussian laser beam," *J. Physique* **43** 1503-1508 (1982).

17.- J. Calatroni and G. Da Costa, "Interferometric determination of the surface profile of a liquid heated by a laser beam," *Opt. Comm.* **42** 5-9 (1982).

18.- G. N. Maracas, G. L. Harris, C. A. Lee and R. A. McFarlane, "On the origin of periodic surface structure of laser-annealed semiconductors," *App.Phys.Lett.* **33**(5), 453-455 (1978).

19.- Z. Guosheng, P.M. Fauchet and A.E. Siegman, "Growth of spontaneous periodic surface structures on solids during laser illumination," *Phys.Rev.B* **26**(10), 5366-5381 (1982).

20.- M.J. Soileau, "Ripple structures associated with ordered surface defects in dielectrics," *IEEE Journal of Quantum Electronics* **20**(5), 464-467 (1984).

21.- T.R. Anthony and H.E. Cline, " Surface rippling induced by surface-tension gradients during laser surface melting and alloying," *J.Appl.Phys.* **48**(9), 3888-3894 (1977).

22.- V. N. Tokarev and V. I. Konov, "Supression of thermocapillary waves in laser melting of metals and semiconductors," *J.Appl.Phys.* **76**(2), 800-805 (1994).

23.- F. Vega, N. Lupon, J. Armengol, and F. Laguarta, "Laser application for optical glass polishing," *Opt. Eng.* **37**, 272-279 (1998).